Wideband High-Speed and High-Accuracy Instantaneous Frequency Measurement System

Chongjia Huang, Erwin Hoi Wing Chan, *Senior Member, IEEE*, Peng Hao, and Xudong Wang

***Abstract*—A new photonic-assisted instantaneous frequency measurement system is presented. It overcomes the latency problem in the reported structures based on the frequency-to-time mapping technique or the frequency-to-power mapping technique that involves a long length of fiber, and at the same time, enables the incoming microwave signal frequency to be measured over a wide frequency range with only small errors. The system generates three low-frequency signals. The phases of the three low-frequency signals are compared. One of the two low-frequency signal phase differences is used to estimate the incoming microwave signal frequency unambiguously over a wide frequency range and the other is used to provide accurate microwave signal frequency measurement. A proof-of-concept experiment is set up. Experimental results show, by measuring the phase difference of two low-frequency signals, the frequency of the input microwave signal can be determined unambiguously in 15 GHz and 500 MHz frequency ranges with errors below ±220 MHz and ±10 MHz respectively. Hence, by using two low-frequency signal phase differences, the input microwave signal frequency can be determined accurately over a wide frequency range. The new photonic-assisted frequency measurement system has a fast response time, which is an order of magnitude shorter than that of the systems based on the frequency-to-time mapping technique and the frequency-to-power mapping technique with a kilometer-long fiber.**

***Index Terms*—Optical signal processing, microwave measurement, fiber optics links and subsystems, radio frequency photonics.**

I. Introduction

MANY applications require measuring the frequency of a microwave signal. An electrical spectrum analyzer can be used to accomplish this task. It has a wide frequency measurement range of few kHz to above 100 GHz and high accuracy. However, an electrical spectrum analyzer is operated based on the frequency scanning technique. Hence the system latency is dependent on the local oscillator sweeping speed, which is in the orders of milliseconds. In applications such as electronic warfare, a microwave signal frequency needs to be captured instantaneously, so that a jammer can be tuned rapidly to jam against a frequency hopping signal [1].

Instantaneous frequency measurement systems are commercially available [2], [3]. Frequency measurement systems from AKON have a 2-18 GHz operating frequency range, 5 MHz measurement accuracy and 300 ns processing time [3]. Photonics provides a solution for wide frequency measurement range, immunity to electromagnetic interference (EMI) and small size. Many photonic-assisted frequency measurement systems have been developed in the past 15 years. The systems based on sweeping the wavelength of an optical source [4] or the frequency of a reference signal [5], [6] use the same principle as an electrical spectrum analyzer. Hence they have the latency problem and are not suitable for electronic warfare applications. The system that involves a delay line loop takes around 100 μs for measuring a microwave signal frequency up to 20 GHz [7]. The recent reported frequency-to-time mapping based frequency measurement systems have a measurement time of around 10 μs [8], [9], [10], [11]. This is still much longer than the processing time of the commercial instantaneous frequency measurement systems.

There are a number of frequency measurement systems operated based on the frequency-to-power mapping technique that involve a kilometer-long fiber [12], [13], [14]. Using a long length of fiber for frequency measurement not only increases the system size but the system time delay is in the order of tens of microseconds. Hence a photonic-assisted frequency measurement system with a fast measurement time cannot be implemented using a frequency-to-time mapping technique or a frequency-to-power mapping technique that involves a long length of fiber. It is worth to point out that although the frequency-to-time mapping based frequency measurement systems have the latency problem, they have multiple frequency measurement capability and small errors. Also note that it is not necessary for a frequency-to-power mapping based frequency measurement system to have a long length of fiber [15], [16], [17], [18]. However, most frequency-to-power mapping based frequency measurement systems have over ±100 MHz measurement errors, which is much larger than that of the commercial instantaneous frequency measurement systems. They also require high-speed photodetectors.

Recently there is a report on a frequency measurement system based on the frequency-to-phase mapping technique [19]. It has a simple and compact structure, and does not have the latency problem. However, the frequency measurement error is in the range of ±200 MHz, which is two orders of magnitude larger

Manuscript received 28 February 2023; revised 30 March 2023; accepted 11 April 2023. Date of publication 14 April 2023; date of current version 26 April 2023. *(Corresponding author: Erwin Hoi Wing Chan.)*

Chongjia Huang and Peng Hao are with the Photonics Information Innovation Center and Hebei Provincial Center for Optical Sensing Innovations, College of Physics Science & Technology, Hebei University, Baoding 071002, China (e-mail: 1286660746@qq.com; haopenghbu@163.com).

Erwin Hoi Wing Chan is with the Faculty of Science and Technology, Charles Darwin University, Darwin, NT 0909, Australia (e-mail: erwin.chan@cdu.edu.au).

Xudong Wang is with the Guangdong Provincial Key Laboratory of Optical Fiber Sensing and Communications, Institute of Photonics Technology, Jinan University, Guangzhou 510632, China (e-mail: txudong.wang@email.jnu.edu.cn).

Digital Object Identifier 10.1109/JPHOT.2023.3267143

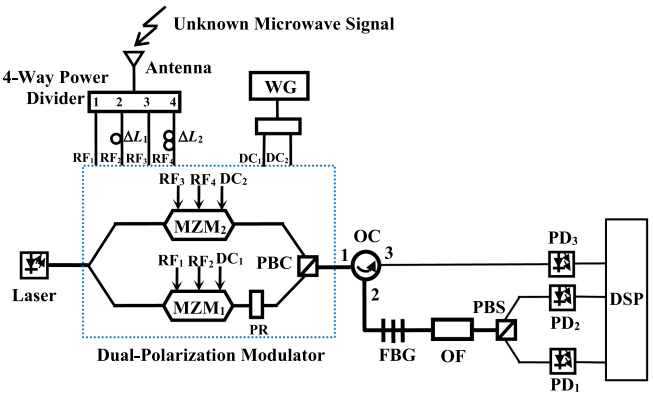

Fig. 1. Topology of the wideband high-speed and high-accuracy instantaneous frequency measurement system. The bold lines represent polarization maintaining components.

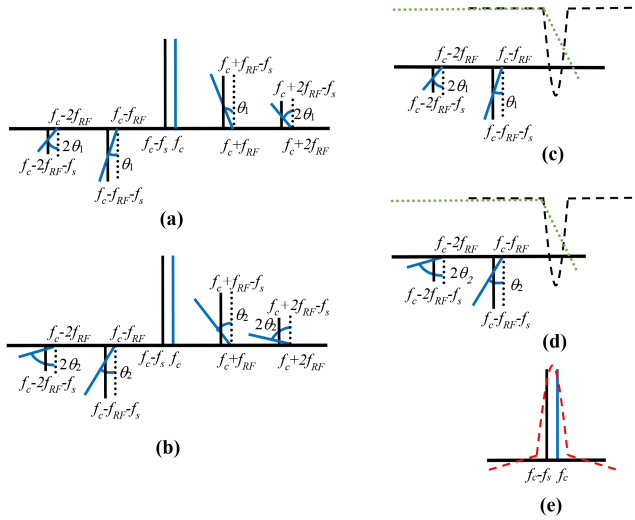

Fig. 2. Spectra at the output of (a) MZM_1 and (b) MZM_2. Spectra of the optical signals into (c) PD_1, (d) PD_2 and (e) PD_3. FBG transmission (black dashed line) and reflection (red dashed line) magnitude response, and OF magnitude response (green dotted line).

than that of the commercial frequency measurement systems [2], [3]. This prevents the frequency-to-phase mapping based frequency measurement system to be used in practice. In this paper, we present an instantaneous frequency measurement system that has a fast measurement time, a large frequency measurement range and small frequency measurement errors. The system uses two pairs of delay lines to produce two low-frequency (LF) signal phase differences. One of the signal phase differences is used for coarse signal frequency estimation over a wide frequency range without ambiguity and the other is used for fine frequency estimation. Experimental results are presented that demonstrate the concept of using two pairs of delay lines and two LF signal phase differences can determine the input microwave signal frequency accurately over a wide frequency range.

II. Topology and Operation Principle

Fig. 1 shows the structure of the proposed wideband high-speed and high-accuracy instantaneous frequency measurement system. A laser source generates a continuous wave (CW) light, which is traveled in the slow axis of a polarization maintaining fiber (PMF) before launching into an optical modulator. The optical modulator is a dual-polarization binary phase shift keying (BPSK) dual-drive Mach-Zehnder modulator (Fujitsu FTM7980EDA). It comprises a 3 dB coupler, two BPSK modulators, a 90° polarization rotator (PR) and a polarization beam combiner (PBC). Each BPSK modulator has two input RF ports and a DC port. An unknown microwave signal received by an antenna is equally split into four portions via a 4-way power divider. The four microwave signals at the power divider outputs are applied to the RF ports of the two BPSK modulators. As shown in the figure, the power divider Port 1 and 2 are connected to the two RF ports (RF_1 and RF_2) of the lower BPSK modulator (MZM_1). Note that there is a length difference ΔL_1 between the two electrical paths. Similarly, the power divider Port 3 and 4 are connected to the two RF ports (RF_3 and RF_4) of the upper BPSK modulator (MZM_2) with a path length difference ΔL_2. The DC port of the two BPSK modulators are driven by a LF ramp waveform from a waveform generator (WG). The peak-to-peak amplitude of the ramp waveform is twice the BPSK modulator DC port switching voltage. This results in shifting the frequency of the light traveled in one arm of the BPSK modulator [20], [21]. The amount of the frequency shift is the same as the input ramp waveform frequency, which can be 50 kHz for example. MZM_n output electric field is given by

$$\begin{aligned} E_{MZMn}(t) = \frac{E_{in}\sqrt{t_{ff}}}{2\sqrt{2}} e^{j\omega_c t} \{ & J_0(\beta_{RF})\left(e^{-j\omega_S t}+1\right) \\ & + J_1(\beta_{RF})\left[-e^{-j\omega_{RF} t}(e^{-j\omega_S t}+e^{j\theta_n}) \right. \\ & \left. + e^{j\omega_{RF} t}(e^{-j\omega_S t}+e^{-j\theta_n})\right] \\ & + J_2(\beta_{RF})\left[-e^{-j2\omega_{RF} t}(e^{-j\omega_S t}+e^{j2\theta_n}) \right. \\ & \left. + e^{j2\omega_{RF} t}(e^{-j\omega_S t}+e^{-j2\theta_n})\right]\} \end{aligned} \quad (1)$$

where E_{in} and ω_c are the electric field amplitude and the angular frequency of the CW light into the dual-polarization modulator respectively, t_{ff} is the insertion loss of the dual-polarization modulator, $J_m(x)$ is the Bessel function of mth order of the first kind, $\beta_{RF} = \pi V_{RF}/V_{\pi,RF}$ is the modulation index, V_{RF} is the amplitude of the unknown microwave signal received by the antenna into the modulator, $V_{\pi,RF}$ is the modulator RF port switching voltage, ω_S and ω_{RF} are the angular frequency of the ramp waveform and the unknown microwave signal respectively, $\theta_n = \omega_{RF}\Delta\tau_n + \theta_e$, $\Delta\tau_n$ is the signal time delay due to the electrical path length difference ΔL_n, and θ_e is the phase imbalance of the 4-way power divider used to split the incoming microwave signal. The spectra at the output of MZM_1 and MZM_2 are shown in Fig. 2(a) and (b) respectively. Note from the figure that the optical carriers at f_c-f_s and f_c have the same phase whereas the sidebands with and without frequency shift have a phase difference depending on the time delay. Also note that ΔL_1 and ΔL_2 shown in Fig. 1 are different. Hence the two signal time

delays ($\Delta\tau_1$ and $\Delta\tau_2$) are different and consequently $\theta_1 \neq \theta_2$. The polarization state of the optical signal at the output of MZM_1 is rotated by 90° via a PR. The two orthogonally polarized optical signals traveled in the two arms of the dual-polarization modulator are combined via a PBC. The electric field of the optical signal at the output of the dual-polarization modulator is given by

$$E_{DPol-MZM}(t) = E_{MZM1}(t)\,\hat{x} + E_{MZM2}(t)\,\hat{y} \quad (2)$$

where $\hat{x}$ and $\hat{y}$ represent the two orthogonally polarized optical signal polarization states.

The x- and y-polarization state optical signals are traveled in the fast and slow axis of a PMF and are launched into an optical circulator (OC), a fiber Bragg grating (FBG), an optical filter (OF) and a polarization beam splitter (PBS) as shown in Fig. 1. The center frequency of the FBG is the same as the laser source frequency. Hence the optical carriers are reflected by the FBG while the sidebands pass through the FBG. The OF filters out the upper sidebands. The two orthogonally polarized optical signals, which contain the lower sidebands, are split by the PBS. The x- and y-polarization optical signals from MZM_1 and MZM_2 are detected by LF photodetectors (PD_1 and PD_2) respectively. The electric fields of the optical signals into PD_1 and PD_2 can be written as

$$\begin{aligned} &E_{out1}(t) \\ &= \frac{E_{in}\sqrt{t_{ff}}}{2\sqrt{2}} e^{j\omega_c t}\left\{-J_1(\beta_{RF})e^{-j\omega_{RF}t}(e^{-j\omega_S t} + e^{j\theta_1})\right. \\ &\left.-J_2(\beta_{RF})e^{-j2\omega_{RF}t}(e^{-j\omega_S t} + e^{j2\theta_1})\right\} \end{aligned} \quad (3)$$

$$\begin{aligned} &E_{out2}(t) \\ &= \frac{E_{in}\sqrt{t_{ff}}}{2\sqrt{2}} e^{j\omega_c t}\left\{-J_1(\beta_{RF})e^{-j\omega_{RF}t}(e^{-j\omega_S t} + e^{j\theta_2})\right. \\ &\left.-J_2(\beta_{RF})e^{-j2\omega_{RF}t}(e^{-j\omega_S t} + e^{j2\theta_2})\right\} \end{aligned} \quad (4)$$

The optical carriers reflected by the FBG are routed from Port 2 to Port 3 of the OC into another LF photodetector (PD_3). Therefore the electric field of the optical signal into PD_3 can be expressed as

$$E_{out3}(t) = \frac{E_{in}\sqrt{t_{ff}}}{2\sqrt{2}} e^{j\omega_c t} J_0(\beta_{RF})\left(e^{-j\omega_S t} + 1\right)[\hat{x} + \hat{y}] \quad (5)$$

The spectra of the optical signals into PD_1, PD_2 and PD_3 are shown in Fig. 2(c)–(e) respectively. The optical signals with and without frequency shift are beat at the LF photodetectors (PD_1, PD_2 and PD_3). This generates photocurrents with the frequency same as the input ramp waveform frequency. The photocurrents at the output of PD_n, which is the product of the photodetector responsivity $\Re$ and the system output electric field square, can be expressed as

$$\begin{aligned} &I_{PD1}(t) = \frac{P_{in}t_{ff}}{4}\Re \\ &\sqrt{J_1(\beta_{RF})^4 + J_2(\beta_{RF})^4 + 2J_1(\beta_{RF})^2 J_2(\beta_{RF})^2 \cos 3\theta_1} \\ &\times \cos(\omega_S t + \phi_1) \end{aligned} \quad (6)$$

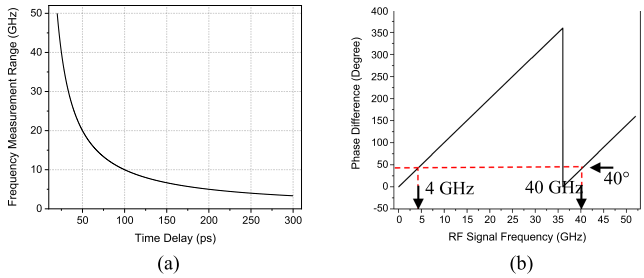

Fig. 3. (a) Frequency measurement range of the proposed structure versus the time delay between two microwave signals into a BPSK dual-drive MZM inside the dual-polarization modulator. (b) Phase difference between the signals at PD_3 and PD_1 outputs versus the input microwave signal frequency, when $\Delta\tau_1 = 27.8$ ps.

$$\begin{aligned} &I_{PD2}(t) = \frac{P_{in}t_{ff}}{4}\Re \\ &\sqrt{J_1(\beta_{RF})^4 + J_2(\beta_{RF})^4 + 2J_1(\beta_{RF})^2 J_2(\beta_{RF})^2 \cos 3\theta_2} \\ &\times \cos(\omega_S t + \phi_2) \end{aligned} \quad (7)$$

$$I_{PD3}(t) = \frac{P_{in}t_{ff}}{2}\Re J_0(\beta_{RF})^2 \cos(\omega_S t) \quad (8)$$

where P_{in} is the power of the CW light into the dual-polarization modulator and

$$\phi_n = \tan^{-1}\left(\frac{-\left(J_1(\beta_{RF})^2 \sin\theta_n + J_2(\beta_{RF})^2 \sin 2\theta_n\right)}{J_1(\beta_{RF})^2 \cos\theta_n + J_2(\beta_{RF})^2 \cos 2\theta_n}\right) \quad (9)$$

The photocurrents are fed into a digital signal processor (DSP), which performs phase comparison between the three LF signals. According to (6)–(8), the phase difference between the LF signals at PD_3 and PD_1 output is $-\phi_1$, and the phase difference between the LF signals at PD_3 and PD_2 output is $-\phi_2$. Under the small signal modulation condition, the second order sidebands are small, which can be neglected. Under an ideal situation, the power divider has no phase imbalance. Hence, according (9), the phase difference $-\phi_1$ is $\theta_1 = 2\pi f_{RF}\Delta\tau_1$ and the phase difference $-\phi_2$ is $\theta_2 = 2\pi f_{RF}\Delta\tau_2$. Therefore the frequency of the unknown microwave signal into the system can be determined by either $-\phi_1$ or $-\phi_2$.

III. Simulation Results and Discussion

In practice, a phase detector can only measure a signal phase difference within 0°–360°. Therefore the electrical path length difference needs to be designed to obtain a time delay that results in a one-to-one mapping between a phase shift within 0°–360° and a microwave signal frequency in a given frequency measurement range. Fig. 3(a) shows the relationship between the frequency measurement range and the required signal time delay. As shown, the larger the frequency measurement range the smaller the time delay is needed. A 36 GHz frequency measurement range requires a time delay of 27.8 ps. Fig. 3(b) shows a unique mapping between a 4–40 GHz microwave signal frequency and a phase difference of 0°-360°, when the system

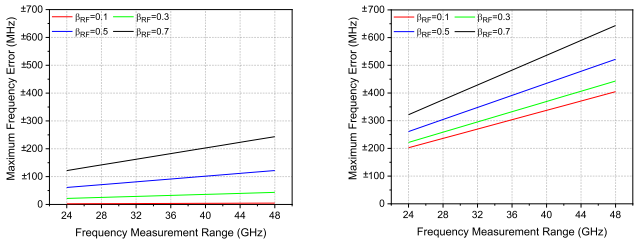

Fig. 4. (a) Maximum amount of frequency measurement error caused by the second order sidebands and (a) 0° and (b) ±3° power divider phase imbalance, versus the frequency measurement range.

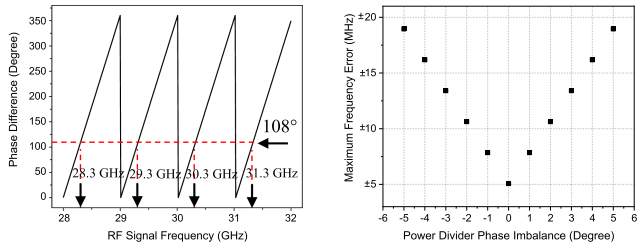

Fig. 5. (a) Phase difference between the signals at PD_3 and PD_2 outputs versus the input microwave signal frequency, and (b) maximum amount of frequency measurement error versus the power divider phase imbalance, when $\Delta\tau_2 = 1$ ns and $\beta_{RF} = 0.7$.

is operated under the small signal modulation condition, the power divider has no phase imbalance, and $\Delta\tau_1 = 27.8$ ps. In this case, for every 100 MHz change in the microwave signal frequency, there is a 1° change in the phase difference, which can be measured using a field programmable gate array (FPGA) based phase detector [22].

Note from Fig. 2(c) and (d) that, in addition to the first order sidebands, there are second order sidebands into the photodetectors. The second order sideband amplitude is dependent on the incoming microwave signal power, which is unknown. The presence of the second order sidebands causes the phase difference to deviate from θ_1, which consequently causes deviation in the phase difference to microwave signal frequency relationship from that shown in Fig. 3(b). This leads to errors when determining the incoming microwave signal frequency using the phase difference. Another major cause of frequency measurement error in the proposed structure is the power divider phase imbalance θ_e. The frequency measurement error f_e is given by

$$f_e = \frac{\phi_n}{2\pi\Delta\tau_n} - f_{RF} \tag{10}$$

Fig. 4 shows the maximum amount of frequency measurement error, obtained using the phase difference of the LF signals at PD_3 and PD_1 outputs, for different frequency measurement ranges. As can be seen from Fig. 4(a), for a frequency measurement range of 36 GHz, which is realised by using a time delay of 27.8 ps, the frequency measurement error, caused by the presence of the second order sidebands, is within ±180 MHz for a modulation index of less than 0.7. As shown in Fig. 4(b), with the inclusion of ±3° power divider phase imbalance, the maximum amount of frequency measurement error is increased from ±180 MHz to ±480 MHz for the system having a 36 GHz frequency measurement range.

Fig. 4 shows the frequency measurement error is small when the system is designed to have a small frequency measurement range. As the frequency measurement range increases, the error also increases. This indicates that a wide measurement range and a high measurement accuracy cannot be achieved at the same time. This limitation is present in many reported photonic-assisted frequency measurement systems. In the proposed structure, two different time delays ($\Delta\tau_1$ and $\Delta\tau_2$) are used to produce two phase differences ($-\phi_1$ and $-\phi_2$). The time delays $\Delta\tau_1$ is designed to provide a coarse microwave signal frequency measurement over a wide frequency measurement range while $\Delta\tau_2$ is designed so that the microwave signal frequency can be measured accurately. For example, as shown in Fig. 3, the time delay $\Delta\tau_1 = 27.8$ ps is needed to measure a microwave signal frequency over the 4–40 GHz frequency range. According to Fig. 4(b), the frequency measurement error for the system with a 36 GHz frequency measurement range can be ±480 MHz. Hence the time delay $\Delta\tau_2$ is designed to be 1 ns to provide a fine frequency measurement within a 1 GHz frequency measurement range, which is more than twice the maximum frequency measurement error of ±480 MHz for $\Delta\tau_1 = 27.8$ ps. The corresponding phase difference to microwave signal frequency relationship and the maximum frequency measurement error versus the power divider phase imbalance are shown in Fig. 5. This shows a small frequency measurement error of less than ±13 MHz can be obtained for a power divider phase imbalance of less than ±3° and a modulation index below 0.7. This is a 36-time improvement in frequency measurement accuracy compared to that when using only one time delay of 27.8 ps for 4–40 GHz frequency measurement.

Assuming the incoming microwave signal frequency is 29.3 GHz, for $\Delta\tau_2 = 1$ ns, the phase difference $-\phi_2$ is $2\pi\Delta\tau_2 f_{RF} = 10548°$. Since a phase detector can only measure a phase difference between 0° and 360°, a phase difference of 10548° corresponds to 108° displayed on a phase detector under an ideal situation. Due to the presence of the second order sidebands and ±3° power divider phase imbalance, the phase difference $-\phi_2$ obtained from the phase detector is within 108° ± 4.7°. Hence, according to Fig. 5, the estimated incoming microwave signal frequency obtained from the phase difference $-\phi_2$ is ($k \times 1$ GHz) + 0.3 GHz with a maximum error of ±13 MHz, where k is an integer. The incoming microwave signal frequency is also estimated using the phase difference $-\phi_1$ obtained from another phase detector in the DSP and $\Delta\tau_1 = 27.8$ ps, and it is 29.3 GHz ± 480 MHz. This shows k can only be 29 in order for the estimated microwave signal frequency obtained from $-\phi_2$ to be within the 29.3 GHz ± 480 MHz frequency range. Therefore, by using the two phase differences ($-\phi_1$ and $-\phi_2$) at the system output, a microwave signal frequency can be measured over a wide frequency range with small errors. For $\Delta\tau_2 = 1$ ns and using a phase detector with a phase detection

resolution of 1°, the frequency of a microwave signal can be measured with a resolution of 2.8 MHz. Hence the proposed structure also has a high frequency measurement resolution. Since the proposed frequency measurement system determines the incoming microwave signal frequency by measuring the signal phase differences, a phase detection error causes an error in frequency measurement. However, a phase detector can be made to have a high accuracy of better than 0.1° [23]. Hence the frequency measurement error caused by the phase detector detection error can be neglected.

The 1 dB compression point of the proposed frequency measurement system, which is defined as the input microwave signal power required to cause the loss of the output LF signal to increase by 1 dB, can be obtained from (6). It is between 6.9 dBm to 8.8 dBm for 0° to 360° phase difference. The proposed frequency measurement system has a wide frequency measurement range where the upper operating frequency is only limited by the power divider bandwidth. 2–40 GHz 4-way power dividers are commercially available. They have a typical phase imbalance of ±2.8° [24]. A wideband DC-67 GHz 4-way power divider [25] can be used in the proposed structure for microwave frequency measurement beyond the Ka band. The system lower operating frequency is determined by the reflection bandwidth of the FBG used to reflect the optical carriers, which can be made to be few GHz. The proposed frequency measurement system has a fast measurement time as it does not require sweeping a laser wavelength or a reference signal frequency, and does not involve a long length of fiber or use the frequency-to-time mapping technique.

IV. Experimental Results

An experiment was set up similar to that shown in Fig. 1 to demonstrate the concept of the high-speed and high-accuracy instantaneous frequency measurement system. A tunable laser (Keysight N7711A) generated a CW light, which passed through a polarization controller (PC) into a dual-polarization BPSK dual-drive MZM (Fujitsu FTM7980EDA). Due to the lack of a 4-way power divider, a 2-way power divider was used to split a microwave signal from a 20 GHz microwave signal generator. The microwave signal at each power divider output passed through a phase shifter, which had an adjustable length of 6 mm. The output of one of the phase shifters was connected to a 30 mm connector adaptor. This results in a 30 mm with ±6 mm adjustable electrical path length difference between the two electrical paths from the power divider to the RF ports of MZM_1 in the dual-polarization modulator. A 50 kHz ramp waveform from a waveform generator was applied to MZM_1 DC port. The peak-to-peak amplitude of the ramp waveform was set to be 11.6 V, which is two times the modulator DC port switching voltage, to introduce 50 kHz frequency shift on the optical signal traveled in one arm of MZM_1. The RF ports of MZM_2 were terminated by 50 Ω terminators. A DC voltage was applied to MZM_2 DC port to bias MZM_2 at the null point. The output of the dual-polarization BPSK dual-drive MZM was connected to an OC, a FBG, a tunable optical bandpass filter and a PBS as shown in Fig. 1. The reflection magnitude response of the

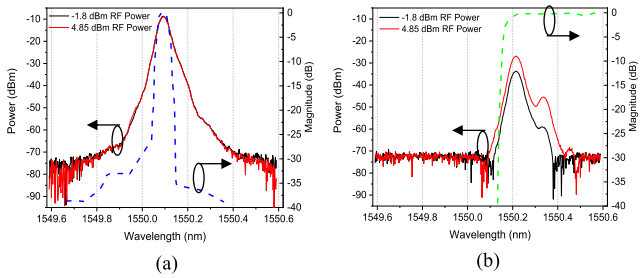

Fig. 6. Measured optical spectra at (a) the OC Port 3 and (b) one of the PBS output ports when a 15 GHz microwave signal with a power of −1.8 dBm (black line) and 4.85 dBm (red line) into MZM_1. The blue dashed line is the normalised reflection magnitude response of the FBG. The green dashed line is the normalised magnitude response of the tunable optical bandpass filter.

FBG is shown in Fig. 6(a). As shown, the FBG has a center wavelength of 1550.1 nm, a narrow 3-dB reflection bandwidth of 8.5 GHz and a stopband rejection level of around 35 dB. A PC was connected to the tunable optical bandpass filter output. It was adjusted so that the x-polarization optical signal from MZM_1 and the y-polarization optical signal from MZM_2 were routed to two different PBS output ports.

The tunable laser wavelength was set at the FBG center wavelength. A microwave signal at 15 GHz frequency from the microwave signal generator was applied to the dual-polarization modulator. The center wavelength and the bandwidth of the tunable optical bandpass filter were adjusted so that the optical filter has a magnitude response as shown in Fig. 6(b) to filter out the lower sidebands in wavelength, which corresponds to the upper sidebands in optical frequency. The optical spectra at the OC Port 3 and at the output of the PBS that contains the optical signal from MZM_1 were measured on an optical spectrum analyzer. They are shown in Fig. 6(a) and (b) for two different microwave signal powers of −1.8 dBm and 4.85 dBm into the modulator. Since the RF port of MZM_1 has a switching voltage of around 3 V, the modulation indexes are 0.28 and 0.58 for the two input microwave signal powers. As shown in the figures, the optical carriers are reflected by the FBG (Fig. 6(a)) while the upper sidebands in wavelength are passed through the FBG and the tunable optical bandpass filter (Fig. 6(b)). Fig. 6(b) also shows the optical carrier is largely suppressed, and for a modulation index of less than 0.58, the second order sideband is more than 18.7 dB below the first order sideband.

The carriers and sidebands shown in Fig. 6 were amplified by erbium-doped fiber amplifiers (EDFAs) before detecting by two photodetectors (PD_1 and PD_3) (Discovery Semiconductor DSC30S). The optical signals with and without 50 kHz frequency shift beat at the photodetectors. A 50 kHz LF signal was generated at each photodetector output. It was amplified by a LF electrical amplifier followed by a 50 kHz lowpass filter (LPF) for eliminating the harmonic components. The two amplified 50 kHz signals were injected into an FPGA based DSP, which has an LCD display showing the input signal phase difference. Due to the FBG used in the experiment has a 3-dB reflection bandwidth of 8.5 GHz and the microwave signal generator available for experiment has a bandwidth of 20 GHz, microwave signal frequency measurement can only be demonstrated in a frequency range of 5 to 20 GHz. Hence the length of the phase shifter was

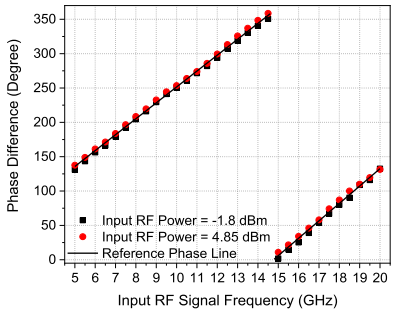

Fig. 7. Phase difference between the two system output 50 kHz signals generated by PD_3 and PD_1 for different microwave signal frequencies of 5–20 GHz into MZM_1.

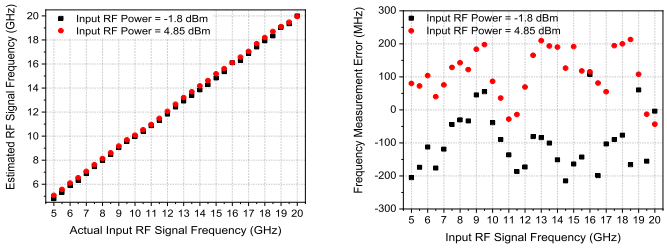

Fig. 8. (a) Estimated microwave signal frequency versus actual input microwave signal frequency. (b) Frequency measurement errors at different input microwave signal frequencies. The signal time delay $\Delta\tau_1$ is 67 ps.

adjusted so that the time delay of the two electrical signals into MZM_1 was 67 ps to obtain a unique mapping between 5–20 GHz input microwave signal frequency and 0°-360° output LF signal phase difference. Fig. 7 shows the phase difference measured on the DSP when the input microwave signal frequency was changed from 5 to 20 GHz with a step of 0.5 GHz. As shown, the phase difference has a linear relationship with the microwave signal frequency. More importantly, each microwave signal frequency within the 5–20 GHz frequency range has a unique phase difference. The figure also shows a reference phase line, which was obtained using the time delay introduced by the two electrical path length difference and a constant phase shift introduced by the LF electrical components connected to the photodetector output.

The input microwave signal frequency can be estimated using the phase difference measured on the DSP and the reference phase line. It is shown in Fig. 8(a). The difference between the estimated microwave signal frequency and the actual frequency of the microwave signal into the system is the frequency measurement error, which is shown in Fig. 8(b). As shown, the frequency measurement error is less than $\pm$220 MHz for a microwave signal with different frequencies between 5–20 GHz and different powers of -1.8 dBm and 4.85 dBm into the system. The error is mainly caused by the phase detection error from the DSP and the power divider phase imbalance. Since the DSP only measures the phase difference of two system output LF signals and there is only little change in the power divider phase imbalance over the 5–20 GHz frequency range, the frequency measurement error does not increase with the input microwave signal frequency as can be seen in Fig. 8(b).

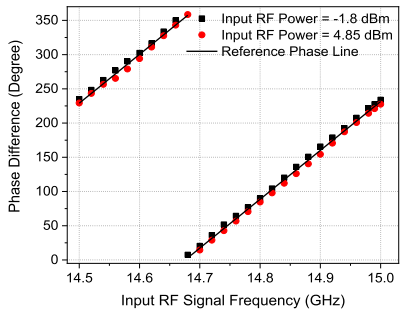

Fig. 9. Phase difference between the two system output 50 kHz signals generated by PD_3 and PD_2 for different microwave signal frequencies of 14.5–15 GHz into MZM_2.

To demonstrate the frequency measurement error can be reduced by designing the signal time delay, the microwave signal and the 50 kHz ramp waveform were applied to MZM_2 instead of MZM_1. A short length of electrical cable was inserted to one of MZM_2 RF ports to introduce a time delay $\Delta\tau_2 = 2$ ns to realise a 500 MHz frequency measurement range, which is more than twice the frequency measurement error of $\pm$220 MHz for $\Delta\tau_1 = 67$ ps. This results in a unique mapping between a microwave signal frequency of 0 to 500 MHz and a phase difference of 0° to 360°. This frequency to phase difference mapping relationship is repeated for every 500 MHz. The upper sidebands generated by MZM_2 passed through the OC, the FBG, the tunable optical bandpass filter, the PC and the PBS. They were amplified by an EDFA before detecting by a photodetector (PD_2). The optical carriers reflected by the FBG were routed from Port 2 to Port 3 of the OC into an EDFA and a photodetector (PD_3). As before, the 50 kHz LF signal generated by the photodetector was amplified by the 1 MHz bandwidth amplifier and passed through the 50 kHz LPF before injecting into the FPGA based DSP.

Fig. 9 shows the system output 50 kHz signal phase difference measured by the DSP, for a microwave signal with different frequencies of 14.5 to 15 GHz and different powers of -1.8 dBm and 4.85 dBm into MZM_2. A one-to-one mapping between a microwave signal frequency of 14.5–15 GHz and 0°–360° phase difference can be seen. Note that the phase difference measurement shown in Fig. 9 was obtained by increasing the input microwave signal frequency from 14.5 to 15 GHz with a step of 20 MHz. As shown in the figure, there is an around 14° phase change for every 20 MHz change in the input microwave signal frequency. This agrees with the phase difference to time delay relationship stated in Section II. Phase detectors with an accuracy of better than 1° and a phase detection range of 0°–360° have been reported [22], [23], [26]. Hence the input microwave signal frequency can be measured in high resolution by using these high-accuracy phase detectors in the proposed structure. As before, an estimated microwave signal frequency can be obtained using the measured phase difference and the reference phase line. It is shown in Fig. 10(a). Fig. 10(b) shows the frequency measurement error, which is the difference between the estimated and actual input microwave signal frequency, is within $\pm$10 MHz. This shows the frequency measurement error is reduced from $\pm$220 MHz to $\pm$10 MHz when the frequency measurement range is reduced from 15 GHz to 500 MHz.

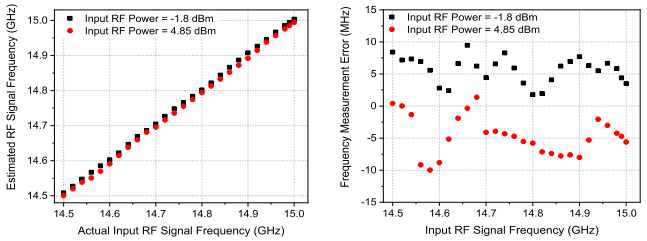

Fig. 10. (a) Estimated microwave signal frequency versus actual input microwave signal frequency. (b) Frequency measurement errors at different input microwave signal frequencies. The signal time delay $\Delta\tau_2$ is 2 ns.

The experimental results show, the proposed structure, which produces two LF signal phase differences ($-\phi_1$ and $-\phi_2$), can determine the input microwave signal frequency over a wide frequency range with small errors.

The input microwave signal frequency was fixed at 15 GHz. The phase difference displayed on the phase detector was recorded every 5 minutes over an hour. The measurement shows the phase difference has less than $\pm 0.5^\circ$ change throughout the one-hour measurement period. This shows the proposed frequency measurement system has a stable performance. The noise components in the system are the laser relative intensity noise, the signal-spontaneous beat noise, the shot noise and the thermal noise. The signal-spontaneous beat noise from the EDFA was found to be the dominant noise component in the system. The noise floor of the system was more than 80 dB below the LF signal at the phase detector input for an input microwave signal power of -1.8 dBm. It was found that the frequency measurement error increases as the input microwave signal power reduces to below -5 dBm. This is because, for a -5 dBm input microwave signal power, the power of the LF signal generated by the beating of the two first order sidebands at the photodetector is below 0 dBm, which is outside the DSP operating power range. The EDFA gain needs to be increased or a LF electrical amplifier with a higher gain needs to be used before the DSP in order for the frequency measurement system to operate at small input microwave signal powers.

The time delay for the microwave signal traveled from the power divider input to the photodetector output was measured to be 218 ns. It was mainly due to the instrument EDFA used in the setup, which has a time delay of around 130 ns. Phase detectors with a fast response time of around 1 μs have been reported [26], [27]. Using these phase detectors in the proposed structure to measure the LF signal phase differences, the incoming microwave signal frequency can be determined with an order of magnitude faster than the systems based on the frequency-to-time mapping technique and the frequency-to-power mapping technique with a kilometer-long fiber. This overcomes the latency problem in the reported photonic-assisted frequency measurement systems [4], [5], [6], [7], [8], [9], [10], [11], [12], [13], [14]. Table I shows the performance comparison of the proposed and reported frequency measurement systems without the latency problem. As shown, most of the reported instantaneous frequency measurement systems have simple structures.

TABLE I
PERFORMANCE COMPARISON OF THE PROPOSED AND REPORTED FREQUENCY MEASUREMENT SYSTEMS

Reference	Measurement Range (GHz)	Measurement Error (MHz)	System Complexity	Integrable
[15]	0.5-17.5	±200	Moderate	No
[16]	9-19	±150	Low	No
[17]	1-18	±200	Low	Yes
[18]	4.4-8.7	±200	Low	Yes
[19]	5-20	±200	Low	Yes
[28]	6-18	±300	Low	Yes
[29]	0.5-36	±200	Low	No
[30]	1-10	±200	Low	Yes
[31]	0.04-40	±1950	Moderate	Yes
[32]	1-10	-	Moderate	Yes
This work	5-20	±10	Moderate	Yes

However, they have high frequency measurement errors of above ±100 MHz. Note that recently there are few reports on frequency measurement systems implemented using integrated photonic technology that have fast measurement times [33], [34]. They operated based on the original frequency-to-power mapping technique, which requires a pair of high-speed photodetectors. The system output microwave signal powers are measured, which are used to construct an amplitude comparison function (ACF) for estimating the incoming microwave signal frequency. The integrated photonics based frequency measurement systems have an over 30 GHz frequency measurement range and root mean square errors of 755 MHz [33] and 10.85 MHz [34].

V. CONCLUSION

A wideband, high-speed and high-accuracy instantaneous frequency measurement system has been presented. It is based on using two signal time delays in a microwave photonic structure to generate two LF signal phase differences. One of the signal phase differences is used to estimate the incoming microwave signal frequency unambiguously over a wide frequency range. The other is used to provide accurate estimation on the microwave signal frequency. The proposed instantaneous frequency measurement system overcomes the latency problem in many reported photonic-assisted frequency measurement systems. It also has high frequency measurement resolution and a compact structure, which can be implemented using off-the-shelf components or integrated photonic technology. Experimental results demonstrate, by using a signal time delay of 67 ps (2 ns) and measuring the phase difference of two system output LF signals, the input microwave signal frequency can be determined unambiguously in a 5 to 20 GHz (14.5 GHz to 15 GHz) frequency range with errors below ±220 MHz (±10 MHz). Hence the proposed structure, which has two different time delays and produces two LF signal phase differences, can determine the input microwave signal frequency accurately over a wide frequency range. A short optical signal time delay of 218 ns and a high frequency measurement resolution of 20 MHz have also been demonstrated. The proposed instantaneous frequency measurement system should find application in modern electronic warfare and electronic countermeasure systems.

REFERENCES

[1] D. C. Schleher, *Electronic Warfare in the Information Age*. Norwood, MA, USA: Artech House, 1999.

[2] "2 to 18 GHz Instantaneous frequency measurement unit (DR058) datasheet," 2023. [Online]. Available: https://www.teledynedefenseelectronics.com/

[3] "Digital frequency discriminator 2.0 - 18.0 GHz (A55-MH024) datasheet," 2023. [Online]. Available: https://www.akoninc.com/

[4] T. Hao, J. Tang, W. Li, N. Zhu, and M. Li, "Microwave photonics frequency-to-time mapping based on a Fourier domain mode locked optoelectronic oscillator," *Opt. Exp.*, vol. 26, no. 26, pp. 33582–33591, 2018.

[5] S. Zheng, S. Ge, X. Zhang, H. Chi, and X. Jin, "High-resolution multiple microwave frequency measurement based on stimulated Brillouin scattering," *IEEE Photon. Technol. Lett.*, vol. 24, no. 13, pp. 1115–1117, Jul. 2012.

[6] H. Jiang et al., "Wide-range, high-precision multiple microwave frequency measurement using a chip-based photonic Brillouin filter," *Optica*, vol. 3, no. 1, pp. 30–34, 2016.

[7] T. A. Nguyen, E. H. W. Chan, and R. A. Minasian, "Instantaneous high-resolution multiple-frequency measurement system based on frequency-to-time mapping technique," *Opt. Lett.*, vol. 39, no. 8, pp. 2419–2422, 2014.

[8] J. Shi, F. Zhang, Y. Zhou, S. Pan, Y. Wang, and D. Ben, "Photonic scanning receiver for wide-range microwave frequency measurement by photonic frequency octupling and in-phase and quadrature mixing," *Opt. Lett.*, vol. 45, no. 19, pp. 5381–5384, 2020.

[9] L. Wang et al., "Compact multi-tone microwave photonic frequency measurement based on a single modulator and frequency-to-time mapping," *J. Lightw. Technol.*, vol. 40, no. 19, pp. 6517–6522, Oct. 2022.

[10] Y. Wan, X. Fan, B. Xu, and Z. He, "Microwave frequency measurement with high accuracy and wide bandwidth based on whispering-gallery mode barcode," *Opt. Lett.*, vol. 46, no. 19, pp. 5008–5011, 2021.

[11] B. Zhang, D. Zhu, H. Chen, Y. Zhou, and S. Pan, "Microwave frequency measurement based on an optically injected semiconductor laser," *IEEE Photon. Technol. Lett.*, vol. 32, no. 23, pp. 1485–1488, Dec. 2020.

[12] X. Zhang, H. Chi, X. Zhang, S. Zheng, X. Jin, and J. Yao, "Instantaneous microwave frequency measurement using an optical phase modulator," *IEEE Microw. Wireless Compon. Lett.*, vol. 19, no. 6, pp. 422–424, Jun. 2009.

[13] S. Wang, G. Wu, Y. Sun, and J. Chen, "Photonic compressive receiver for multiple microwave frequency measurement," *Opt. Exp.*, vol. 27, no. 18, pp. 25364–25374, 2019.

[14] C. Yang, L. Wang, and J. Liu, "Photonic-assisted instantaneous frequency measurement system based on a scalable structure," *IEEE Photon. J.*, vol. 11, no. 3, Jun. 2019, Art. no. 5501411.

[15] Z. Zhao, K. Zhu, L. Lu, and C. Lu, "Instantaneous microwave frequency measurement using few-mode fiber-based microwave photonic filters," *Opt. Exp.*, vol. 28, no. 25, pp. 37353–37361, 2020.

[16] L. Liu and W. Xue, "Instantaneous microwave frequency measurement based on two cascaded photonic crystal nanocavities," *IEEE Photon. J.*, vol. 12, no. 6, Dec. 2020, Art. no. 4501809.

[17] M. V. Drummond, P. Monteiro, and R. N. Nogueira, "Photonic RF instantaneous frequency measurement system by means of a polarization-domain interferometer," *Opt. Exp.*, vol. 17, no. 7, pp. 5433–5438, 2009.

[18] J. Li, L. Pei, T. Ning, J. Zheng, Y. Li, and R. He, "Measurement of instantaneous microwave frequency by optical power monitoring based on polarization interference," *J. Lightw. Technol.*, vol. 38, no. 8, pp. 2285–2291, Apr. 2020.

[19] C. Huang and E. H. W. Chan, "Microwave frequency measurement based on a frequency-to-phase mapping technique," *Opt. Lett.*, vol. 47, no. 22, pp. 5957–5960, 2022.

[20] L. M. Johnson and C. H. Cox, "Serrodyne optical frequency translation with high sideband suppression," *J. Lightw. Technol.*, vol. 6, no. 1, pp. 109–112, Jan. 1988.

[21] C. Huang and E. H. W. Chan, "Microwave photonic frequency translators with large spurious suppression and wide bandwidth," *IEEE Photon. J.*, vol. 13, no. 2, Apr. 2021, Art. no. 7100409.

[22] J. Mitra and T. K. Nayak, "An FPGA-based phase measurement system," *IEEE Trans. Very Large Scale Integr. Syst.*, vol. 26, no. 1, pp. 133–142, Jan. 2018.

[23] S. J. Lu, P. Siqueira, V. Vijayendra, H. Chandrikakutty, and R. Tessier, "Real-time differential signal phase estimation for space-based systems using FPGAs," *IEEE Trans. Aerosp. Electron. Syst.*, vol. 49, no. 2, pp. 1192–1209, Apr. 2013.

[24] "Minicircuits power splitter/combiner ZC4PD-K0244+," 2017. [Online]. Available: https://www.minicircuits.com/

[25] "Hyperlabs broadband resistive 4-Way power divider HL9577 datasheet," 2022. [Online]. Available: https://www.hyperlabs.com/

[26] R. Liu et al., "FPGA-based amplitude and phase detection in DLLRF," *Chin. Phys. C*, vol. 33, no. 7, pp. 594–598, 2009.

[27] "LF–2.7 GHz RF/IF gain and phase detector (AD8302) datasheet," 2018. [Online]. Available: https://www.analog.com/

[28] J. Dai et al., "A simple photonic-assisted microwave frequency measurement system based on MZI with tunable measurement range and high resolution," *IEEE Photon. Technol. Lett.*, vol. 22, no. 15, pp. 1162–1164, Aug. 2010.

[29] S. Pan and J. Yao, "Instantaneous microwave frequency measurement using a photonic microwave filter pair," *IEEE Photon. Technol. Lett.*, vol. 22, no. 19, pp. 1437–1439, Oct. 2010.

[30] Z. Li, C. Wang, M. Li, H. Chi, X. Zhang, and J. Yao, "Instantaneous microwave frequency measurement using a special fiber Bragg grating," *IEEE Microw. Wireless Compon. Lett.*, vol. 21, no. 1, pp. 52–54, Jan. 2011.

[31] H. Emami, N. Sarkhosh, and M. Ashourian, "Reconfigurable photonic radar warning receiver based on cascaded grating," *Opt. Exp.*, vol. 21, no. 6, pp. 7734–7739, 2013.

[32] N. Sarkhosh, H. Emami, L. Bui, and A. Mitchell, "Microwave photonic instantaneous frequency measurement with improved sensitivity," in *Proc. IEEE Microw. Theory Technol. Soc. Int. Microw. Symp. Dig.*, 2009, pp. 165–168.

[33] M. Burla, X. Wang, M. Li, L. Chrostowski, and J. Azaña, "Wideband dynamic microwave frequency identification system using a low-power ultracompact silicon photonic chip," *Nature Commun.*, vol. 7, 2016, Art. no. 13004.

[34] Y. Tao et al., "Fully on-chip microwave photonic instantaneous frequency measurement system," *Laser Photon. Rev.*, vol. 16, 2022, Art. no. 2200158.